Sennah *et al. Int J Concr Struct Mater (2018) 12:63*
https://doi.org/10.1186/s40069-018-0284-1

International Journal of Concrete Structures and Materials

ORIGINAL ARTICLE

Open Access

Structural Qualification of a Developed GFRP-Reinforced Concrete Bridge Barrier using Ultimate Load Testing

Khaled Sennah[1], Ekaterina Tropynina[1], Zaki Ibrahim[2] and Saman Hedjazi[3*]

Abstract

Corrosion of reinforcing steel bars is the main factor affecting durability and service life of steel-reinforced bridge barriers in North America. The use of glass fiber reinforcing polymer (GFRP) bars as non-corrosive material has emerged as an innovative solution to corrosion related problems. A recent cost-effective design of PL-3 bridge barrier was developed at Ryerson University incorporating high-modulus GFRP bars with headed ends. An experimental program was conducted to investigate the load carrying capacity of the developed barrier wall. A 40-m long barrier was constructed and tested at four different locations to investigate its structural behavior, crack pattern and ultimate strength when subjected to the equivalent static loading simulating vehicle impact. Experimental results were compared with the design values specified in the Canadian Highway Bridge Design Code. Experimental findings showed a large margin of safety for the proposed GFRP-reinforced barriers. The failure pattern due to transversal loading the longitudinal barrier over 2400 mm length was initiated by a trapezoidal flexural crack pattern at front face of the barrier, followed by punching shear failure at the transverse load location. Comparison between the available punching shear equations in the literature and the punching shear failure developed in the barrier wall was conducted.

Keywords: bridge codes and standards, composite material, bridge barrier, glass fiber reinforced polymer (GFRP) bars, full-scale ultimate load testing, punching shear failure

1 Background

In Canada, bridges built prior to the 1970s did not use air-entrained concrete and coated reinforcing steel bars to protect from the effects of freeze–thaw cycles and the application of winter deicing salt. This leads to corrosion-induced degradation in bridges. Accordingly, bridge decks, railings, and barrier walls are all likely candidates for expensive replacement on most of these older bridges. Epoxy-coated reinforcement was developed in the early 1970s as an effective method of corrosion protection. After demonstration projects in the mid 1970s, the use of epoxy-coated bars in highway bridges expanded rapidly and became the preferred method of corrosion protection. The first evidence of unsatisfactory field performance emerged in 1986 in Florida Bridges in USA, with other examples of corrosion of coated reinforcement reported in USA and Canada in the 1990s, especially in bridge barriers (among them: Manning 1996; Smith and Virmani 1996). In de-icing environments, the heavy corrosion to the outer side of the vertical bars in the traffic side of the barrier wall was observed in association with section loss in the horizontal bars after 10–20 years in service. A recent study conducted by Ontario Ministry of Transportation, MTO, (Lai and Raven 2010) revealed that epoxy coating of the steel bars is compromised after certain number of years in service, leading to corrosion and thus concrete cracks and spalling. Later, MTO banned the use of epoxy-coated bars in bridge barriers while allowing the use of noncorrosive glass fiber reinforced polymer (GFRP) bars to promote bridge designs that improve the life expectancy and significantly reduce the maintenance cost of bridges.

*Correspondence: shedjazi@georgiasouthern.edu
[3] Civil Engineering and Construction Department, Georgia Southern University, Engineering Building, Room 1101G, 201 COBA Drive, BLDG 232, Statesboro, GA 30458, USA
Full list of author information is available at the end of the article
Journal information: ISSN 1976-0485 / eISSN 2234-1315

An extensive research program investigating the use of GFRP bars in concrete bridge barrier was carried out by El-Salakawy et al. (2003). In their study, PL-2 and PL-3 bridge barriers with variable geometry, concrete dimensions and reinforcement in accordance with the new Canadian Highway Bridge Design Code were investigated. The study focused on comparing the overall behavior and cracking pattern of barrier walls reinforced with GFRP with that of conventional steel reinforcement under static and impact loadings. Also, El-Salakawy et al. (2005) conducted pendulum impact tests on GFRP-reinforced barriers to examine their crack pattern, stresses and deflection under impact loading.

Few authors dealt with the use of fiber reinforced polymers in concrete barriers. Maheu and Bakht (1994) developed a new barrier wall using GFRP, New Fiber Composite Material for Reinforcing Concrete (NEFMAC) grids, with connection to the deck slab by means of double-headed tension bars of steel spaced at 300 mm. This new barrier wall system was adopted in the Canadian Highway Bridge Design Code (CSA 2006a). El-Salakawy et al. (2003) tested to-collapse PL-2 and PL-3 barrier walls reinforced with low-modulus GFRP bars. They conducted pendulum impact testing (El-Salakawy et al. 2005) on the developed barriers in lieu of vehicle crash testing. In 2007, El-Gamal et al. (2007) conducted pendulum impact testing on PL-2 and PL-3 barrier walls reinforced with GFRP bars with lower tensile strength and bigger modulus of elasticity than those used in the earlier pendulum impact testing. In 2011, Charron et al. (2011) developed a precast bridge parapet made with fibre-reinforced concrete (FRC) using the nonlinear finite-element computer modeling. Specific properties of high- and ultrahigh-performance FRC were exploited in these designs. Others conducted finite-element analysis modeling of GFRP-reinforced bridge barrier (Hedjazi et al. 2016; Khederzadeh and Sennah 2015). They conducted experimental testing on the developed FRC barrier to examine the barrier wall cantilever action and compared the results with numerical simulation. Buth et al. (2003) conducted vehicle crash test on a 685-mm-height bridge open-rail reinforced with glass fibre-reinforced polymer bars. Sennah et al. (2011, 2014) developed GFRP-reinforced PL-3 barriers and crash-tested it using tractor-trailer and then tested under static loading to collapse (Khederzadeh and Sennah 2014). These tested resulted in two MTO Standard Drawings that are currently used by contractors and consulting engineering to bid on MTO bridge projects. Few authors conducted tests on the capacity of barrier–deck junction incorporating GFRP with headed-ends and bars with 180° hooks (Azimi et al. 2014a, b; Rostami et al. 2016). El-Salakawy and Islam (2014) examined experimentally two repair strategies of a GFRP-reinforced concrete bridge barrier damage by vehicle impact. Most recently, American Association of State Highway and Transportation Officials, AASHTO (2009) established bridge guide specifications for GFRP-reinforced concrete bridge decks and traffic railings. However, this guide does not provide procedure for the design of the barrier wall except for the diagonal tension in the deck slab below the barrier–deck junction based on a recent work by Matta and Nanni (2009).

AASHTO-LRFD bridge design specification (AASHTO 2012) specifies equations for the ultimate flexural capacity of the concrete barrier when subjected to transverse impact loading based on the yield-line theory. In the analysis, it was assumed that the yield-line failure pattern occurs within the barrier wall only and does not extend into the deck slab. This means that the deck slab must have sufficient resistance to force the yield-line failure pattern to remain within the barrier wall. AASHTO-LRFD assumes two yield-line failure patterns based on the location of the truck collision with the barrier wall, as shown in Fig. 1. A force F_t distributed over a length L_t as shown in the figure produces the first yield-line failure pattern caused by a truck collision within a wall segment. This interior yield-line pattern is assumed to have three yield lines as shown in Fig. 1a. Two of the yield lines have tension on the inside face of the barrier wall and one yield line has tension on the outside face of the barrier wall. The latter is a vertical crack along the height of the barrier wall at the location of vehicle impact. The second yield-line failure pattern occurs at the end of the barrier wall as produced by a force F_t distributed over a length L_t as shown in Fig. 1b. In this case, there is only one diagonal yield line that produces tension on the inside face of the barrier. This type of yield-line pattern is assumed to occur at bridge barrier ends and at locations of expansion joints. The angle of the inclined yield lines is expressed in terms of the critical length L_c as shown in Fig. 1. Given the fact that GFRP bars behave elastically till failure, the concept of yield-line analysis may not apply to GFRP-reinforced barrier.

2 Proposed GFRP-Reinforced Barrier

Figure C16.2 in the Commentaries of the Canadian Highway Bridge Design Code (CHBDC) (Canadian Standard Association, CSA 2014b) specifies PL-3 barrier dimensions and GFRP bar detailing shown in Fig. 2a. Pendulum impact test were carried out on this barrier (El-Gamal et al. 2007) considering low-modulus GFRP bars with minimum tensile strengths of 590 and 510 MPa for #5 (15 M in Canadian rebar size) and #6 (20 M in Canadian rebar size) straight bars, respectively, and minimum tensile strengths of 390 and 300 MPa for #5 and #6 bent

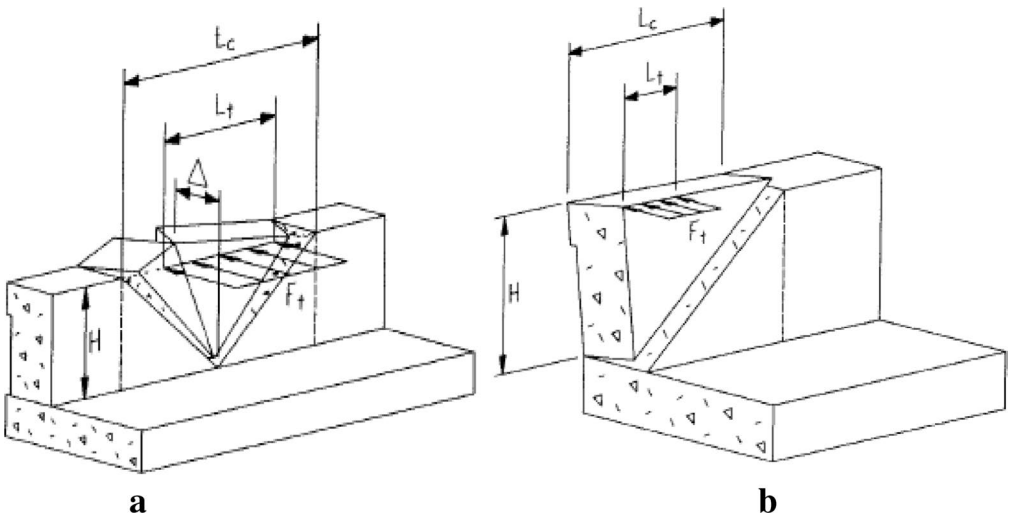

Fig. 1 LRFD yield-line analysis of barrier wall (redrawn from AASHTO 2012). **a** Interior region, **b** end region.

bars, respecstively. Such design is considered outdated given the availability of high-modulus GFRP bars with almost double or more than double the tensile strength of the bars per materials specifications listed by current GFRP manufacturers in Canada.

The GFRP bars used in this paper (SchÖck 2010) have tensile strength of 1188 MPa, compared to 400 MPa yield strength of the currently used reinforcing steel bars as well as the tensile strength for low-modulus GFRP bars mentioned above. The special "ribbed" surface profile of these bars, shown in Fig. 3a, ensure optimal bond between concrete and the bar. Until recently, the installation of GFRP bars was often hampered by the fact that bent bars have to be produced in the factory since GFRP bars cannot be bent at the site. Also, bent GFRP bars are much weaker than straight bars, due to the redirection and associated rearrangement of the fibres in the bend. As a result, number of bent GFRP bars is increased and even doubled at such locations where bar bents are required. In this study, GFRP bars with headed ends are used as straight bars at the inside face of the barrier walls with an end head at the bottom to reduce their development length in the deck slab, avoiding the use of hooks. This headed end is made of a thermo-setting polymeric concrete with a compressive strength far greater than that of normal grade concrete. It is cast onto the end of the straight bar and hardened at elevated temperatures. The concrete mix contains an alkali resistant Vinyl Ester resin, the same material used in the straight bars, and a mixture of fine aggregates. The maximum outer diameter of the end heads is 2.5 times the diameter of the bar. The head of the 16 M diameter bar is approximately 100 mm long. It begins with a wide disk which transfers a large portion of the load from the bar into the concrete. Beyond this disk, the head tapers in five steps to the outer diameter of the blank bar. This geometry ensures optimal anchorage forces and minimal transverse splitting action in the vicinity of the head. It should be noted that the diameters of GFRP bars of 12 and 16 M, used in this study have core (nominal) diameters of 12 and 16 mm, respectively, exterior diameters of 13.5 and 18 mm, respectively, and nominal cross-sectional areas of 113 and 201 m^2, respectively.

The proposed PL-3 barrier shown in Fig. 2b incorporates M16 and M12 GFRP bars as vertical reinforcement in the barrier front and back faces, respectively, at 300 mm spacing. M16 bar was proposed as horizontal reinforcement with bar spacing as shown in Fig. 2b. The connection between the deck slab and the barrier wall utilized the M16 GFRP bars with headed end for proper anchorage. All vertical and diagonal bars in the barrier wall were embedded in the deck slab with 195 mm vertical embedment length. Concrete cover to reinforcement was taken as 50 mm for the barrier wall reinforcement except for the hooked bar at the barrier–deck junction at which the concrete cover was taken as 35 mm.

By comparing the GFRP bar details in CHBDC barrier in Fig. 2a with those in Fig. 2b for the proposed barrier in this research, one may observe the reduction in vertical reinforcement at the front face of the barrier from #6 @ 200 mm to #5 @ 300 mm. Also, the number of horizontal bars changed from 14 to 10. Moreover, the vertical bars at the back face of the barrier was reduced from #5 @ 200 mm to #4 (12 M) @ 300 mm since these bars are always in compression. In addition, there is significant reduction in the length of bars embedded in the deck slab by eliminating the horizontal development length of the

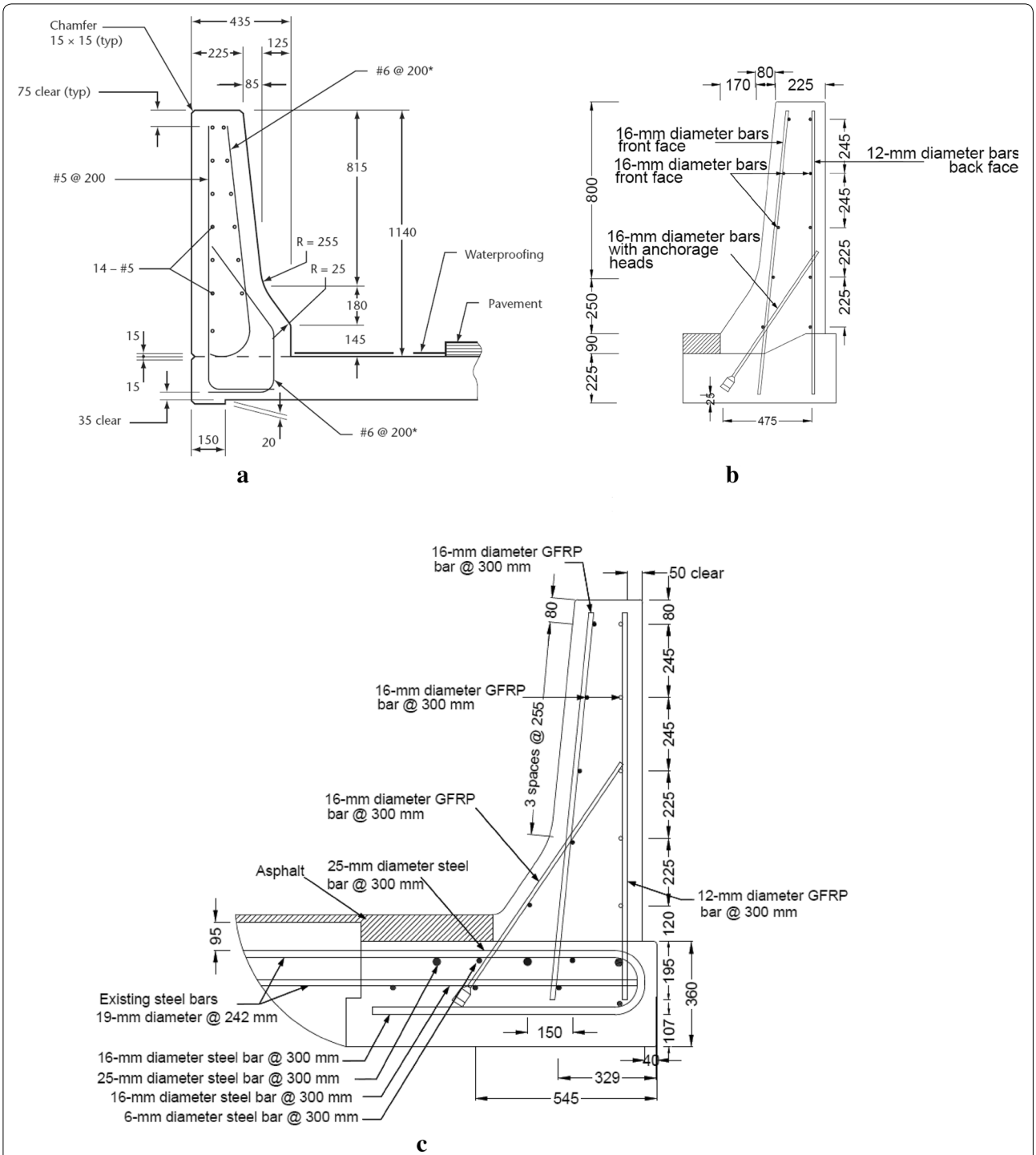

Fig. 2 Schematic diagram of the reinforcement for the proposed barrier and constructed barrier–deck system. **a** CHBDC barrier with low-modulus GFRP bars, **b** proposed barrier with high-modulus GFRP bars, **c** constructed GFRP-reinforced barrier over deck slab cantilever anchored to an existing foundation wall.

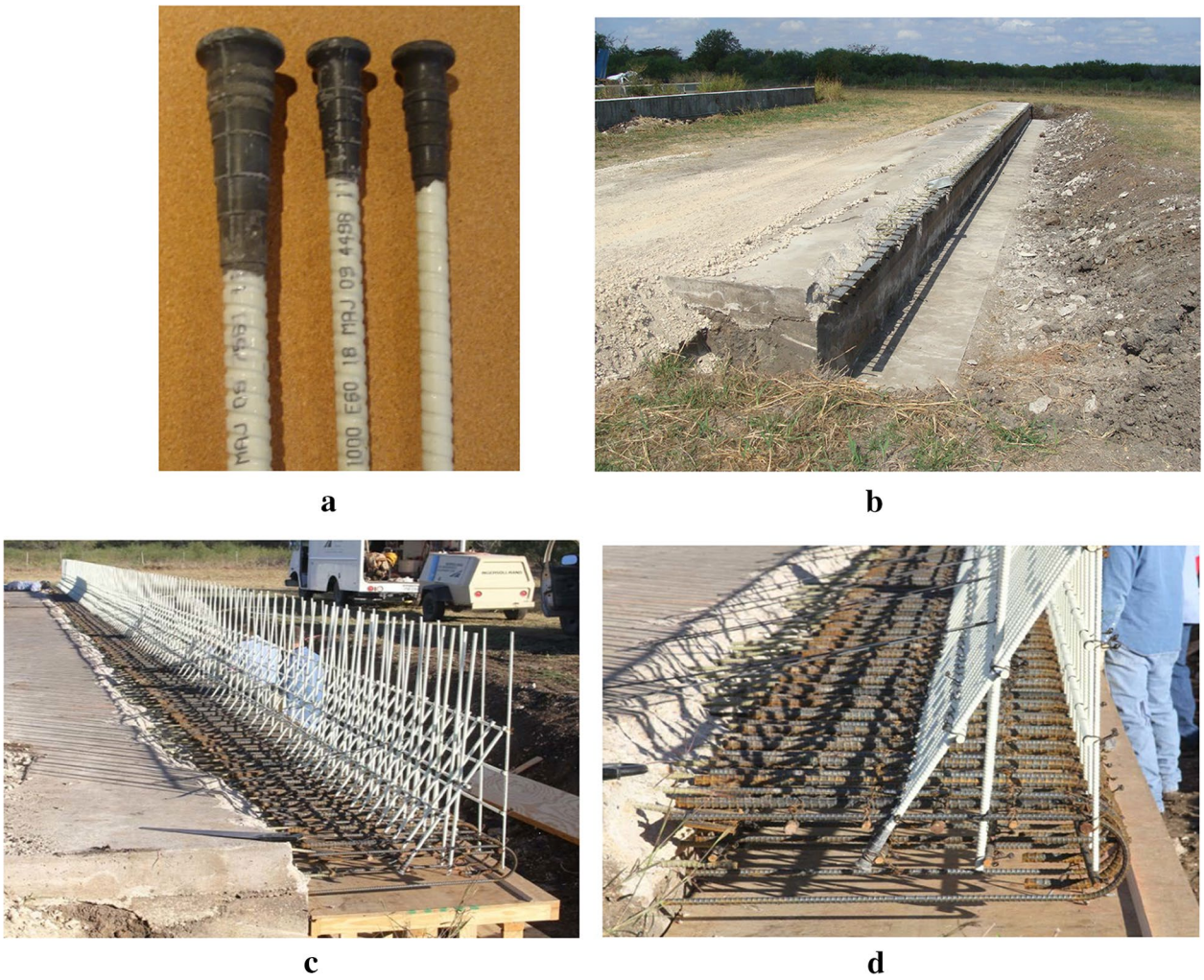

Fig. 3 Views of the GFRP bars, the constructed PL-3 barrier wall and supporting foundation. **a** GFRP bars with cast heads, **b** projecting steel dowels from existing foundation, **c** GFRP reinforcement, **d** deck cantilever reinforcement.

front and back vertical bars, while using bars with headed ends at the extreme tension side of the barrier–deck junction. This will facilitate significant reduction in the manufacturing process by eliminating all bents and horizontal anchorage lengths at the barrier–deck region. Also, the proposed design with high-modulus GFRP bars in Fig. 2b reduces the amount of GFRP bars in the CHBDC barrier detailing in Fig. 2a by about 43%.

CHBDC Clause 12.4.3.4.4 specifies crash testing for the design of the barrier wall itself (i.e. both vertical and horizontal reinforcement). As such, vehicle crash testing was recently conducted to qualify the proposed barrier for use in Canadian bridges. The constructed barrier to perform the crash test was further investigated by conducting static load tests at interior and end locations, which is the subject of this paper.

The design process of bridge barriers is specified in the CHBDC Clause 12.4.3.5 (CSA 2014a) specifies that the suitability of a traffic barrier anchorage to the deck slab shall be based on its performance during crash testing of the traffic barrier. For an anchorage to be considered acceptable, significant damage shall not occur in the anchorage or deck during crash testing. CHBDC also specifies that if crash testing results for the anchorage are not available, the anchorage and deck shall be designed to resist the maximum bending, shear and punching loads that can be transmitted to them by the barrier wall. CHBDC specifies transverse, longitudinal and vertical loads of 210, 70 and 90 kN, respectively, that can be applied simultaneously over a certain barrier length in case of PL-3 barrier. It also specifies that transverse load shall be applied over a barrier length of 2400 mm for PL-3 barriers. Since transverse loading creates the critical

load carrying capacity, both the longitudinal and vertical loads were not considered in the design of barrier wall reinforcement and anchorages between the deck slab and the barrier wall. It should be noted that CHBDC specifies a live load factor of 1.7. Thus, the design impact load on PL-3 barrier wall over 2.4 m length is 357 kN.

When an errant vehicle collides with the bridge barrier, the effect of the lateral impact force is distributed in the barrier and the deck with dispersal angles for interior and end portion of the barrier wall. CHBDC commentaries (CSA 2006b) provided a table for the transverse moment in cantilever slabs due to horizontal railing loads for TL-5 barriers. These factored applied moments were 83 and 102 kN m/m for interior and end portions respectively. These moments were obtained by assuming bridge cantilever of 1.5 m length and for infinite length of the barrier wall. However, the bridge deck slab cantilever may be of different length which is the case of slab-on-girder bridges or the barrier wall can be rigidly fixed to a non-deformable base which is the case of thick solid slab bridges and voided slab bridges. Also, CHBDC Table did provide any further information for designers to obtain design moments for different barrier lengths and slab thicknesses. The length of a barrier is considered between two free ends of the barrier or between expansion joints. Due to limitations of use of these design values, this design tables was omitted from the Commentaries of CHBDC of 2014 (CSA 2014b).

Azimi et al. (2014a, b) conducted parametric study using the finite-element analysis (FEA) modeling, to examine the effects of barrier length, deck slab thickness and cantilever length on the factored applied moment at the barrier–deck junction of PL-3 barrier. They developed the following equations for the factored design moment at the barrier–deck junction as a function of barrier length, L_b, and deck slab cantilever length, L_c, and thickness, t_s, all in meter units. The formulas are applicable only for the range of parameters used for parametric study.

$$M_{internal} = 132 \text{ kN m/m} \quad \text{for fixed base} \tag{1}$$

$$M_{end} = 148 \text{ kN m/m} \quad \text{for fixed base} \tag{2}$$

$$M_{internal} = 100(L_b + 2.3t_s)^{-1} + 2.83t_s^{0.2}(L_b - 1)^{0.7}L_c^{-0.8} + 143t_s + 23 \quad \text{for cantilever slab (internal part)} \tag{3}$$

$$M_{end} = 14t_s^{-1}(L_b + 2.3t_s - 2)^{-1} + 2.83t_s^{0.2}(L_b - 1)^{0.7}L_c^{-0.7} + 240t_s + 25 \quad \text{for cantilever slab (end part)} \tag{4}$$

Equations 1 and 2 are applicable to PL-3 barrier supported over non-deformable base such slab thick solid slab or voided slab bridges. While Eqs. 3 and 4 are applicable to the cantilever portion of the slab-on-girder bridges supporting the PL-3 barrier wall. These moment values can be used to design the barrier–deck junction with respect to vertical bar sizes and spacing, as well as their embedment length in deck slab. In lieu of manual design calculations or when design procedure is unavailable, experimental testing can be considered to qualify the proposed design which is the case in this research for moment at the barrier–deck junction.

3 Experimental Program

A 40-m long barrier wall was built at Texas Transportation Institute with the cross-section configuration and GFRP bar arrangement shown in Fig. 2c. It should be noted that the diagonal GFRP bar at the lower tapered surface of the barrier wall has a headed end embedded in the bridge deck slab to increase its pullout strength due to tensile force resulting from the bending moment at the barrier–deck slab junction. Figure 3 shows views of the GFRP bars forming the barrier wall as well as the steel reinforcement of the cantilever deck slab projecting from an existing foundation at the test site. Figure 4 shows elevation of the barrier wall with 6 control joints, 6 m apart.

Phase 1 of this testing program involved loading the barrier wall with a horizontal line load at a height of 990 mm from the top surface of the concrete deck slab and over 2400 mm length at 3 locations as shown in Fig. 4a. Location 1 is at the end of the barrier wall where the vertical reinforcement (M16 bars) at the front face of the barrier wall was doubled by changing their spacing from 300 to 150 mm over a length of 2500 mm from the end of the barrier wall. Location 2 is at the control joint while location 3 is at the mid-distance between two successive control joints as depicted in Fig. 4a. Phase 2 shown in Fig. 4b involved saw-cutting the barrier wall at interior and end locations to provide a 1000-mm width barrier wall to correlate its experimental moment capacity at the barrier–deck junction with the CHBDC applied factored moment mentioned above. So, phase 3 involved loading this cantilever wall at location 4 (interior location) and location 5 (end location) with a line load of length 1000 mm at a height of 990 mm from top surface of the concrete deck slab as depicted in Fig. 4c. Concrete cylinders taken during concrete casting resulted in concrete characteristic compressive strength of 32 MPa at the time of the testing which was 3 months after casting. In case of locations 1, 2 and 3, Linear Variable Displacement Transducers (LVDTs) were placed at the top of the barrier wall at 1200 mm spacing to measure barrier

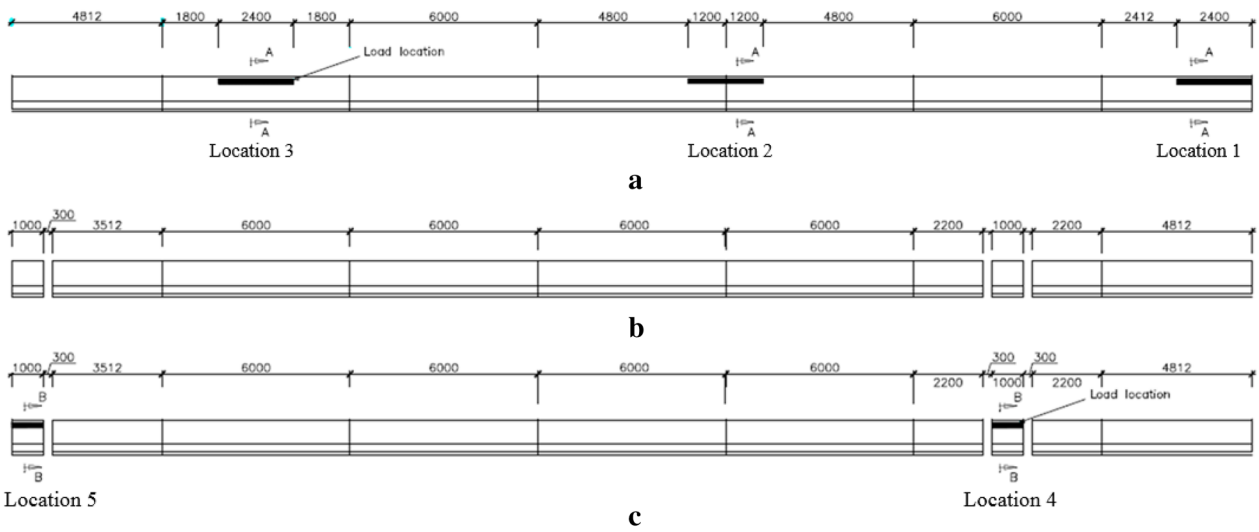

Fig. 4 Schematics diagrams of the barrier showing control joints and applied load locations. **a** Phase 1: loading the barrier wall over 2400 mm length at three locations, **b** phase 2: saw-cut the barrier wall at two locations, **c** phase 3: loading the barrier wall over 1000 mm length at two locations.

lateral deflection, while three LVDTs were placed at the bottom of the deck and oriented vertically to measure deck cantilever deflection during testing. In case, of locations 4 and 5, two LVDTs were placed at the top of the barrier wall at 800 mm spacing to measure barrier lateral deflection, while two LVDTs were placed at the bottom of the deck and oriented vertically to measure deck cantilever deflection during testing.

Figure 5 shows views of the test setup for the loaded segments of the barrier wall. The lateral load was applied using a hydraulic jack of 2500 kN capacity. The jacking load was applied on a steel I-beam oriented horizontally, that transferred that load to two spread beams to form a line load over 2400 mm length of the barrier wall. A trapezoidal timber wedge was inserted between the tapered face of the barrier and the spread beam to ensure that the transferred load acted horizontally on the barrier wall. This load transfer system ensured that a uniformly distributed line load was applied on the barrier wall. The hydraulic jack rest on a steel curved plate attached to a steel column and the push steel beams were rest on a steel table on the front side of the barrier wall. In case of locations 4 and 5, one spread beam was used to apply a load over 1000 mm length of the barrier wall.

4 Test Results and Discussions

Each barrier location was subjected to increasing static load using the jacking system and steel frame. At a load increment of 25 kN, the barrier wall was inspected to mark crack propagation until collapse. The barrier was considered failed when the sensors continued to record increasing deflections with no increase in applied load (i.e. the barrier could not absorb an increase in the applied load). In the following Sects. (4.1 to 4.5) we will discuss test results that are summarized in Table 1.

4.1 Location 1: Barrier Segment at End Location

In this test, the barrier wall was loaded at its end with a line load over 2400 mm length. Figure 6 shows views of the crack pattern after failure. It was observed that with increase in load, horizontal crack appeared at the front side of the barrier wall–deck slab junction. Other horizontal cracks visually appeared on the tapered part of the front side of the barrier wall at a load of 350 kN. These cracks appeared within the 2400 mm length of the line load, extending diagonally outside the loading region and reaching the top surface of the barrier wall at a load of 380 kN. Also, these horizontal cracks propagated through barrier thickness at the end of the barrier wall till reaching an ultimate load of 593 kN. These cracks showed that the barrier wall behaved as a cantilever wall within the 2400 mm length of the line load, while the two-way slab action appeared outside this region (on the left side of the line load) in the form of diagonal cracks extending to the top surface. However, punching shear crack appeared on the left side of the line load at a load of 550 kN and propagated though the barrier thickness and towards the end of the barrier at an ultimate load of 593 kN. The barrier could not absorb any increase in load beyond such load. It can be observed that the crack pattern shown in Fig. 6c

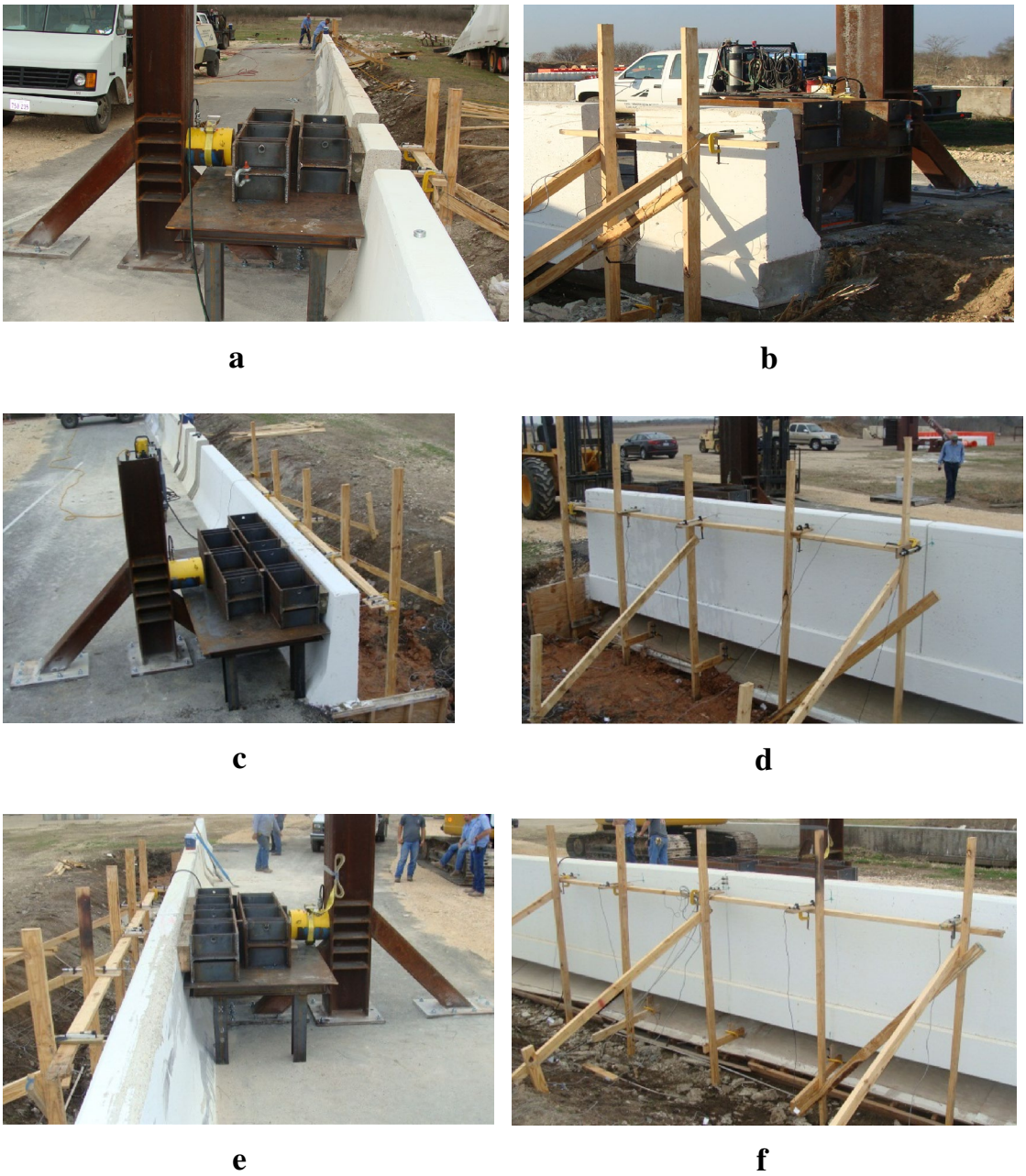

Fig. 5 Views of the test setups for constructed barrier. **a** Test setup for 1000 mm length barrier wall at interior location, **b** test setup for 1000 mm length barrier wall at exterior location, **c** test setup for the barrier wall loaded over 2400 mm length at exterior location, **d** back side of the exterior 2400 mm loaded length showing sensor supporting frame, **e** test setup for the barrier wall loaded over 2400 mm length at interior location, **f** back side of the interior 2400 mm loaded length showing sensor supporting frame.

contradict with the AASHTO-LRFD crack pattern, shown in Fig. 1b where only one diagonal yield line is formed at the front face of the barrier extending from the barrier–deck junction at barrier end diagonally into the barrier wall.

Figures 7 and 8 depict the load–deflection history of the barrier wall and deck slab, respectively. It can be observed that barrier wall has a maximum lateral deflection of 26.43 mm, decreasing to 16.92 mm at the inner side of the line load and 2.43 mm at a 2400 mm distance from the inner side of the line load. According

Table 1 Summary of experimental results.

	Test location[a]				
	Location 1	**Location 2**	**Location 3**	**Location 4**	**Location 5**
First crack (kN)	310	314	320	75	85
Failure load, $F_{failure}$ (kN)	593	607	621	165	189.5
CHBDC factored design load, F_{CHBDC} (kN)	357	357	357	–	–
Height of load application (m)	0.99	0.99	0.99	0.99	0.99
$F_{failure}/F_{CHBDC}$ ratio	*1.66*	*1.70*	*1.74*	–	–
$F_{failure}/F_{CHBDC}$ ratio with 0.75 resistance factor	*1.25*	*1.28*	*1.31*	–	–
Experimental resisting moment, M_{Exp} (kN m/m)	–	–	–	163.35	187.81
CHBDC factored design moment, M_{CHBDC} (kN m/m)	–	–	–	83.00	102.00
M_{Exp}/M_{CHBDC} ratio	–	–	–	*1.97*	*1.84*
M_{Exp}/M_{CHBDC} ratio with 0.75 resistance factor	–	–	–	*1.48*	*1.38*
M_{Exp}/M_{FEA} ratio	–	–	–	*1.53*	*1.32*
M_{Exp}/M_{FEA} ratio with 0.75 resistance factor	–	–	–	*1.15*	*1.0*
Maximum wall deflection (mm)	26.43	11.83	10.83	25.68	26.95
Maximum deck slab cantilever deflection (mm)	9.39	0.61	0.73	4.27	11.76

[a] See Fig. 4 for test locations.

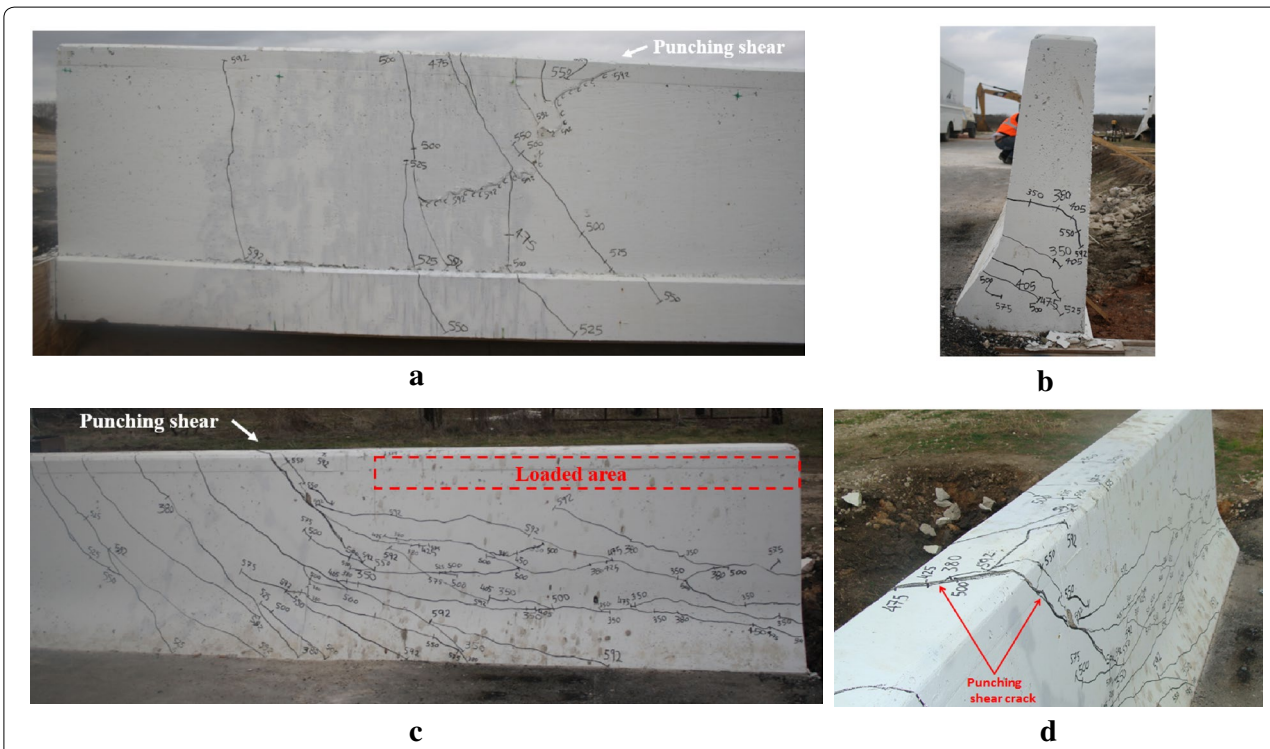

Fig. 6 Crack pattern at end location of the barrier wall. **a** Crack patter at back face of the barrier, **b** flexural cracks at end face of the barrier, **c** crack pattern at front face of the barrier, **d** punching shear through barrier thickness.

to CHBDC of 2006, end portion of PL-3 barrier should resist a factored applied transverse load of 357 kN, which gives a factor of safety of 593/357 = 1.66 in design. Chapter 2 of CHBDC (2014a) specifies that the designer shall consider the environmental conditions and deterioration mechanisms for the FRP reinforcement. Clause 16.4 in Chapter 16 of CHBDC refer to durability of GFRP without considering a value for the durability factor to be taken in design. On the other hand, Clause 16.5.3 specifies resistance factors to be considered in design

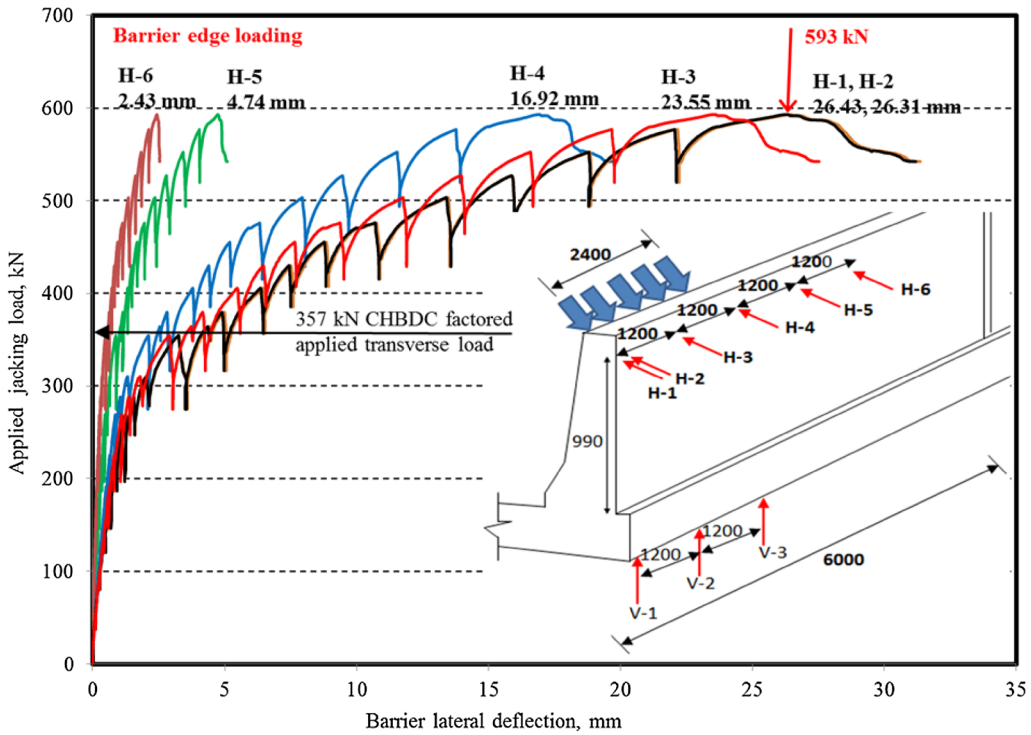

Fig. 7 Load-deflection relationship of the barrier wall loaded at end location.

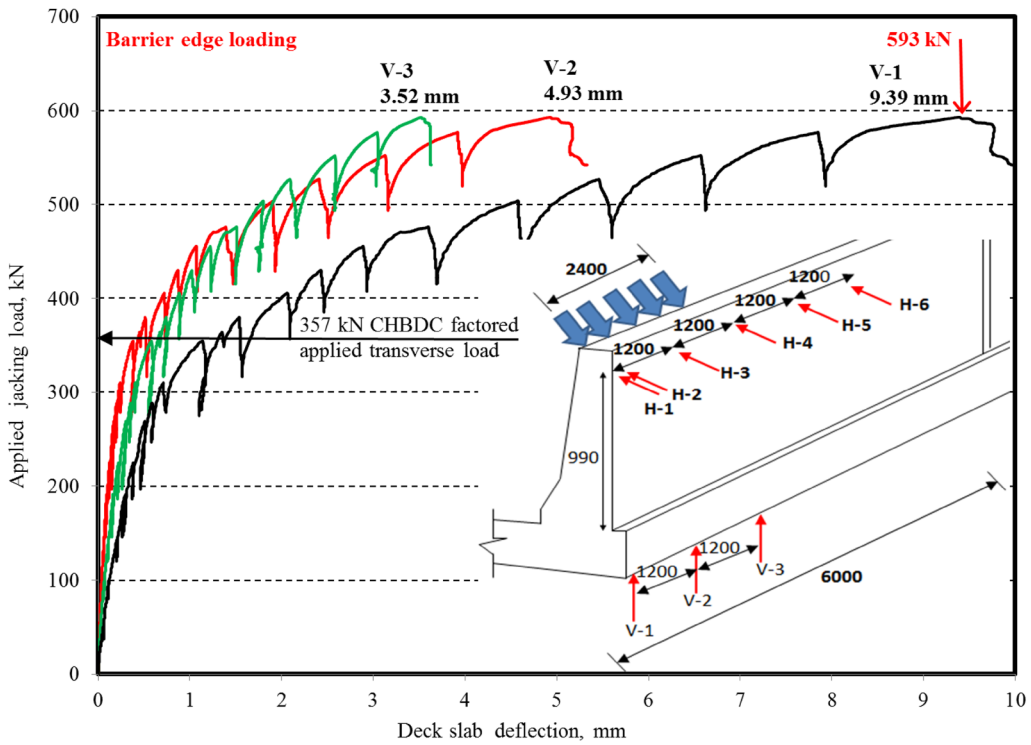

Fig. 8 Load-deflection relationship of the deck cantilever of the barrier wall loaded at end location.

calculations. Such resistance factors are generally associated with uncertainty in material's mechanical properties obtained from standard mechanical test method (i.e. tensile strength test method for example). On the other hand, since the publication of the previous edition of the CHBDC, it is now recognized that the variability of the strength of FRPs is affected more by environmental exposure than by geometric properties and stress levels. It is for this reason that experts in the structural use of FRP are now suggesting that the resistance factors for FRPs should be specified as products of a "material" factor and an "environmental" factor (American Concrete Institute, ACI 440 2002; Karbhari 2000). However, Clause 16.4 in CHBDC commentaries states that findings from analyses of available data in the literature have confirmed that the concerns about the durability of GFRP in alkaline concrete, based on simulated laboratory studies in alkaline solutions, are unfounded. Thus, the resistance factor for design calculations of GFRP in CHBDC was 0.75, as given in CHBDC Commentaries, which was mainly drawn from the Japanese document (Japan Society of Civil Engineers, JSCE 1997). In addition, Clause 16.5.3 in CHBDC of 2006 specified that for bent GFRP bars subjected to vehicular impact loads, the resistance factor for GFRP in design calculations, shall be taken as 0.75 regardless of the method of manufacture. However, this sentence was removed from the 2014 version of the code. Since the scope of this research is to provide experimental findings to qualify the proposed GFRP bar detailing in PL-3 barrier geometries, the experimental factor of safety is considered at least equivalent to 1 to ensure that the experimental capacity is at least equal the CHBDC factored applied transverse loading. In case of using experimental findings to qualify the proposed barrier detailing, the resistance factor for design calculation in nonexistence. However, the authors believe that a generic durability (resistance) factor of 0.75 should apply to the experimental data. As such, the factor of safety for location 1 is $0.75 \times 1.66 = 1.25$.

4.2 Location 2: Barrier Segment at Interior Location and Loaded at the Control Joint

In case of loading the barrier internally at the control joint, Fig. 9 shows views of the barrier wall during testing and the crack pattern after failure. It was observed that with increase in load, horizontal crack appeared at the front side of the barrier wall–deck slab junction. Other horizontal cracks visually appeared on the tapered part of the front side of the barrier wall at a load of 350 kN. These cracks appeared within the 2400 mm length of the line load, extending diagonally outside the loading region and reaching the top surface of the barrier wall at a load

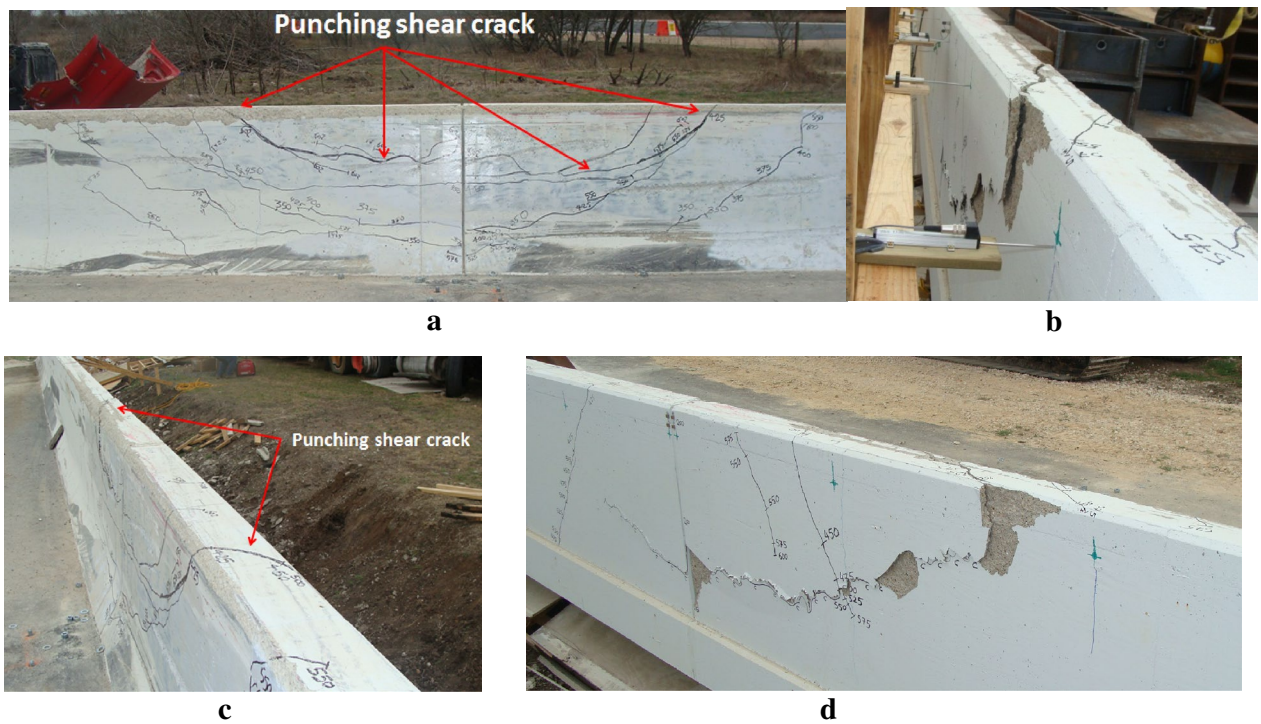

Fig. 9 Views of crack pattern at interior barrier segment loaded at control joint. **a** Crack pattern at front face of the barrier, **b** punching shear through barrier thickness, **c** side view of punching shear failure, **d** back view of punching shear failure.

of 425 kN. These cracks showed that the barrier wall behaved as a cantilever wall within the 2400 mm length of the line load, while the two-way slab action appeared outside this region (on the left and right side of the line load) in the form of diagonal cracks extending to the top surface. However, punching shear crack appeared on the left side of the line load at a load greater than 575 kN and propagated though the barrier thickness and to the other side of the line load at an ultimate load of 607 kN. The sudden punching shear failure at the line load location may be attributed to the GFRP bar low stiffness, bond characteristics, elastic response till failure, low strength under compression and shear stresses. The barrier could not absorb any increase in load beyond 607 kN.

Figures 10 and 11 depict the load–deflection history of the barrier wall and deck slab, respectively. It can be observed that barrier wall has a maximum lateral deflection of 11.04 mm. While the maximum deflection of the deck cantilever at failure of 0.73 mm which is very small indicating the deck slab cantilever was insignificantly affected by the maximum load reached experimentally, promoting the two-way slab action of the barrier wall at the load location. According to CHBDC, PL-3 Barrier should resist a factored applied transverse load of 357 kN, which leads to a factor of safety of 1.7. Considering a resistance factor of 0.75 to the experimental failure load, the factor of safety becomes 1.28.

The crack pattern at this location contradicts with the AASHTO-LRFD crack pattern at interior location shown in Fig. 1a where the two diagonal yield lines at the front face of the barrier meet at the barrier–deck slab junction located at the centre line of the line loading. In addition, a hair vertical crack appeared through the control joint at the back face of the barrier wall at a load of 200 kN. However, this flexural crack did not open enough to form a vertical crack similar to that in yield-line pattern shown in Fig. 1a. This is evident by the horizontal strain readings shown in Fig. 12. To measure the horizontal strains at the back face of the barrier wall, two Pie gauges were installed to the concrete surface at 25 mm from the top surface of the barrier wall and 50 mm apart, as shown in the sketch inserted in Fig. 12. It can be observed that strain readings were insignificant till a load of about 320 kN, then strains increased almost linearly with increase of load till the barrier failed due to punching shear. The recorded strain at failure was in the order of 0.76×10^{-6} which is very small compared to the concrete failure strain of 0.0035.

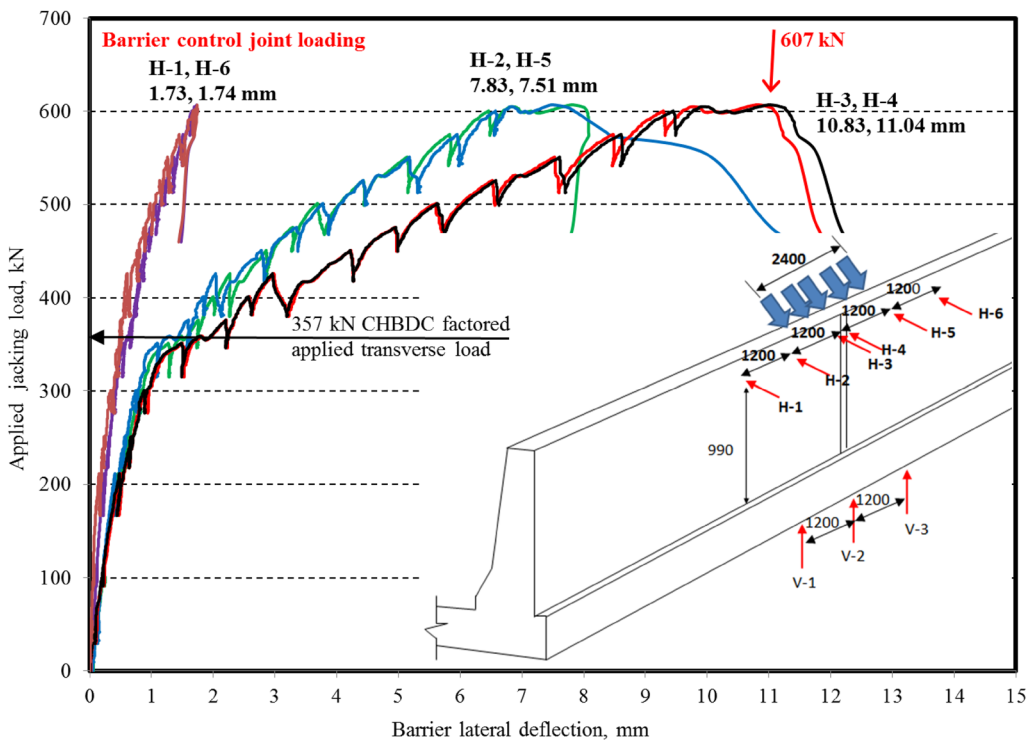

Fig. 10 Load-deflection relationship for barrier segment loaded at control joint.

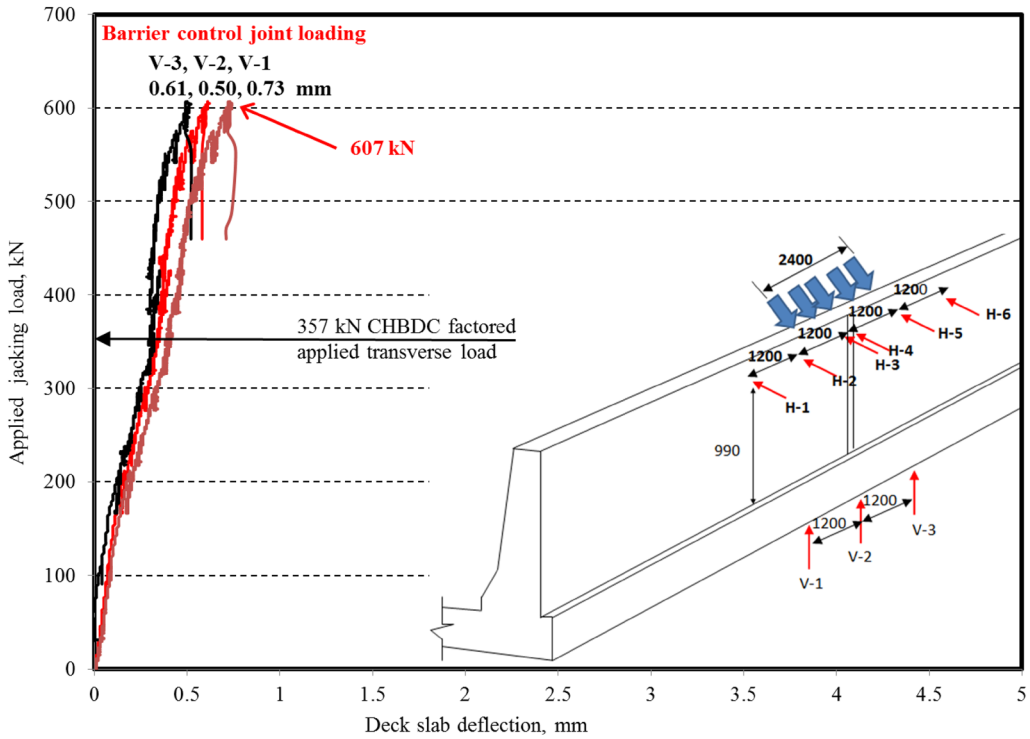

Fig. 11 Load-deflection relationship for the deck cantilever of barrier segment at control joint.

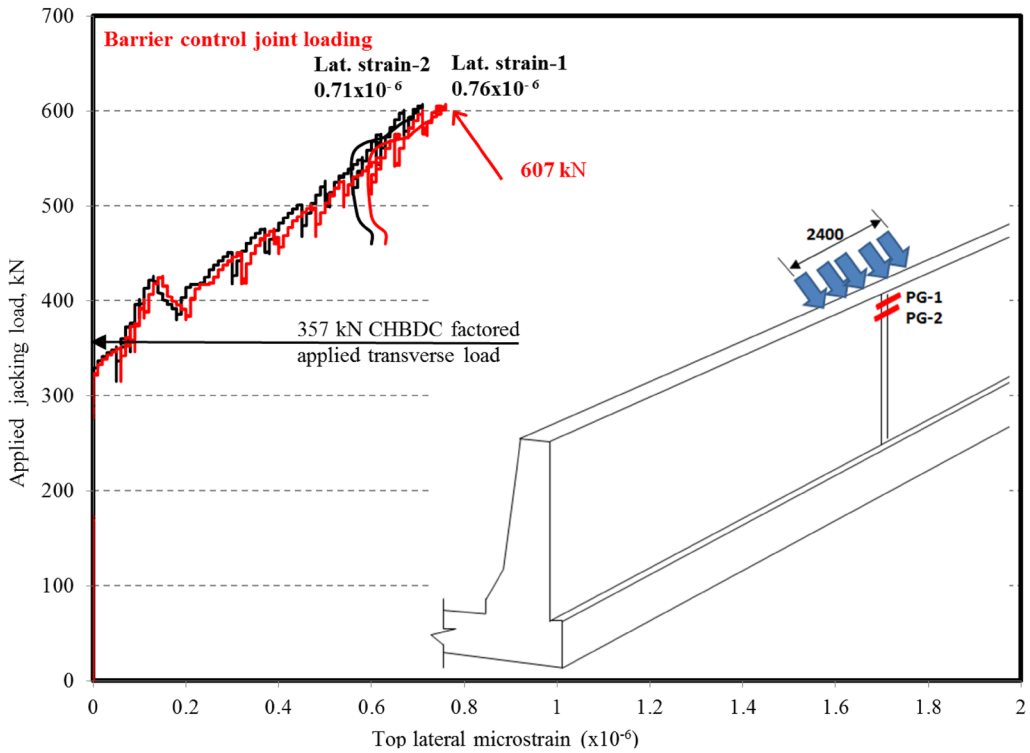

Fig. 12 Load-horizontal strain relationship at the top level of the barrier at control joint.

4.3 Location 3: Barrier Segment at Interior Location and Loaded at Mid-length Between two Successive Control Joints

As for loading the barrier wall at the mid-length between the first and the second control joints shown in Fig. 4a, similar behavior to the loading at the control joint mentioned above was observed. Figure 13 shows views of the crack pattern and failure mode due to punching shear. It was observed that with increase in load, horizontal crack appeared at the front side of the barrier wall–deck slab junction. Other horizontal cracks appeared on the tapered part of the front side of the barrier wall at a load of 300 kN. These cracks appeared within the 2400 mm length of the line load, extending diagonally outside the loading region and reaching the top surface of the barrier wall at a load of 350 kN. These cracks showed that the barrier wall behaved as a cantilever wall within the 2400 mm length of the line load, while the two-way slab action appeared outside this region (on the left and right side of the line load) in the form of diagonal cracks extending to the top surface. However, punching shear crack occurred at the line load location and propagated though the barrier thickness at a load of 600 kN. The barrier could not absorb any increase in load beyond 621 kN.

Figures 14 and 15 depict the load–deflection history of the barrier wall and deck slab, respectively. It can be observed that barrier wall has a maximum lateral deflection of 10.83 mm and a maximum deflection of the deck cantilever at failure of 0.61 mm. According to CHBDC, interior portion of PL-3 barrier should resist factored applied transverse load of 357 kN. This lead to a factor of safety of 1.74 and 1.28 with resistance factor of 1 and 0.75, respectively. It can be observed that the failure load at location 2 where the load was applied at the control joint and location 3 where the load was applied at mid-distance between two consecutive control joints were 607 and 621 kN, respectively. So, the presence of the control joint reduced the load carrying capacity by only 2%.

4.4 Location 4: 1000 mm Cantilever Wall at Interior Location

Figure 16 shows views of the crack pattern in the cantilever wall at interior location after failure.

It can be observed that the first visible flexural crack appeared at the front side of the barrier–deck junction at 75 kN jacking load. The second flexural crack appeared at 105 kN load along the intersection of the two tapered portions of the barrier front face. These cracks propagated through barrier thickness with increase in the applied load. Also, other flexural cracks appeared at the front face of the barrier wall and propagated through the barrier wall thickness with load increase. When the applied load reached 150 kN, extensive cracks appeared in deck slab portion under the barrier wall due to anchorage and diagonal tension, leading to failure of the cantilever wall at 165 kN formation inside the slab. Figure 17 depicts the load–deflection history of the tested wall. One may not consider the importance of the deflection of the barrier and the deck since the design check at the barrier–deck junction is at the ultimate limit state.

This test was intended to examine the flexural capacity of the barrier wall at the bottom of the barrier as well as the anchorage capacity of the barrier–deck junction. Test results showed that the failure load was 165 kN. As such, the associated moment at the barrier wall junction for anchorage capacity is taken as 165 kN × 0.99 m applied load arm to the deck slab = 163.35 kN m/m. According to CHBDC of 2006, the factored applied moment at the barrier deck junction is 83 kN m/m. This leads to a factor of safety of 1.48 with resistance factor of 0.75. However, considering Eq. 3, the factored applied moment at the barrier–deck junction is 106.9 kN m/m, leading to

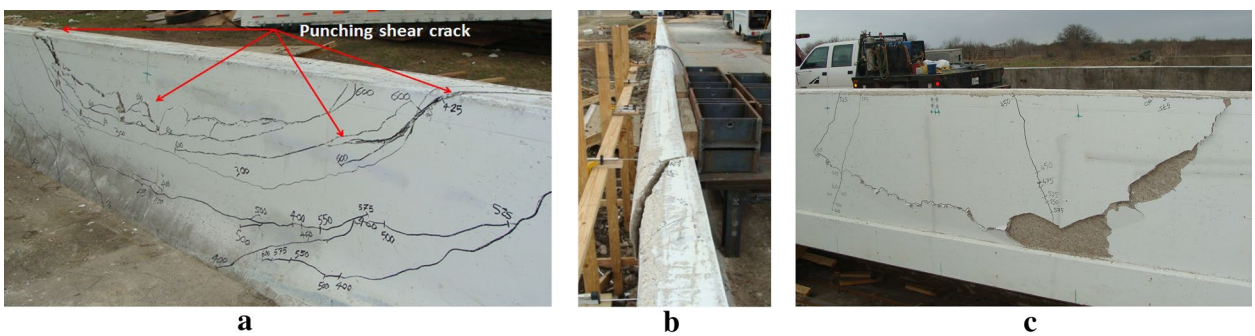

Fig. 13 Views of crack pattern of barrier segment loaded at mid-length between two control joints. **a** Crack pattern at front face of the barrier, **b** wall punching shear, **c** crack pattern at barrier back face.

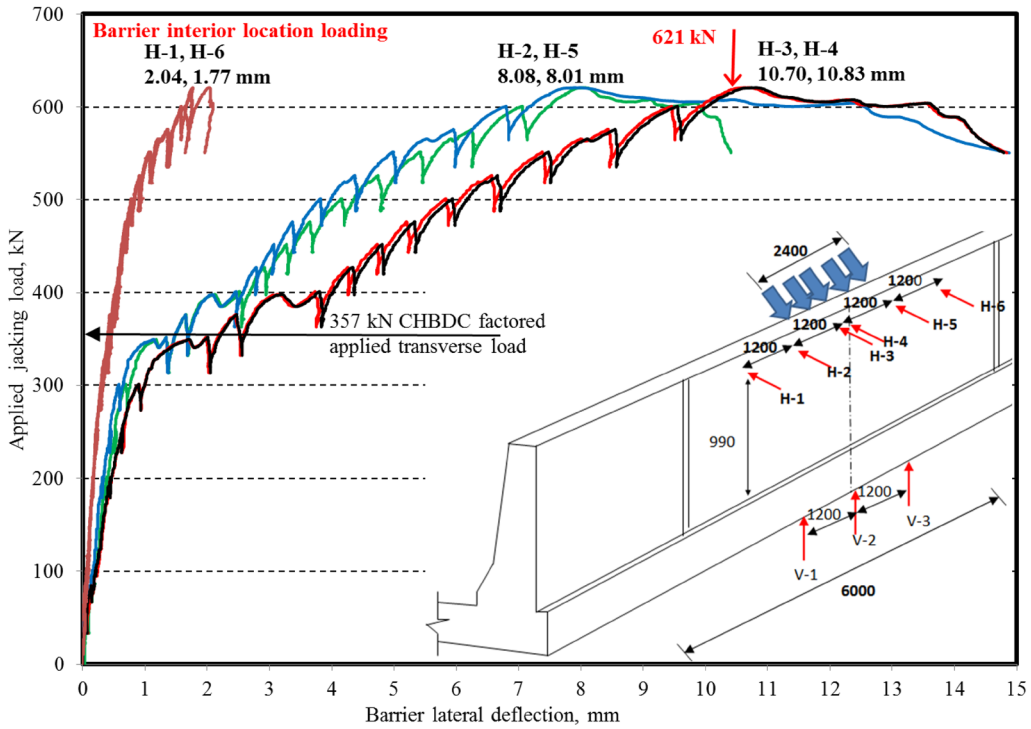

Fig. 14 Load-deflection relationship for barrier segment loaded at mid-length between two control joints.

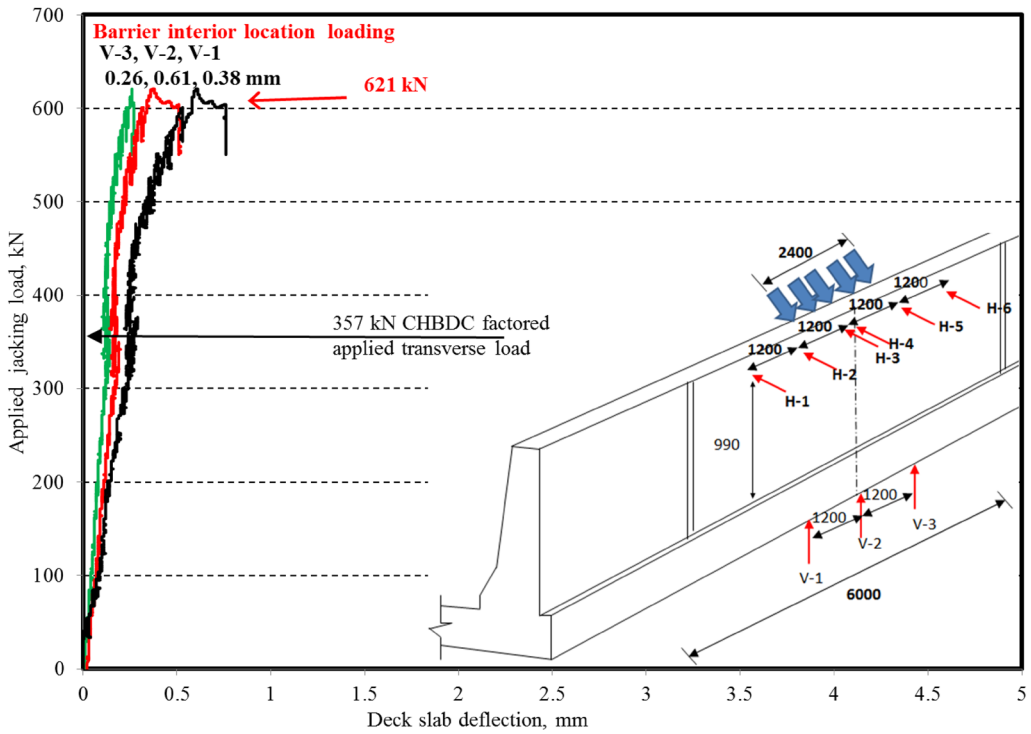

Fig. 15 Load-deflection relationship for the deck cantilever of barrier segment at mid-length between two control joints.

a **b** **c**

Fig. 16 Crack pattern in the 1000 mm length barrier wall at interior location. **a** Left side, **b** right side, **c** front side.

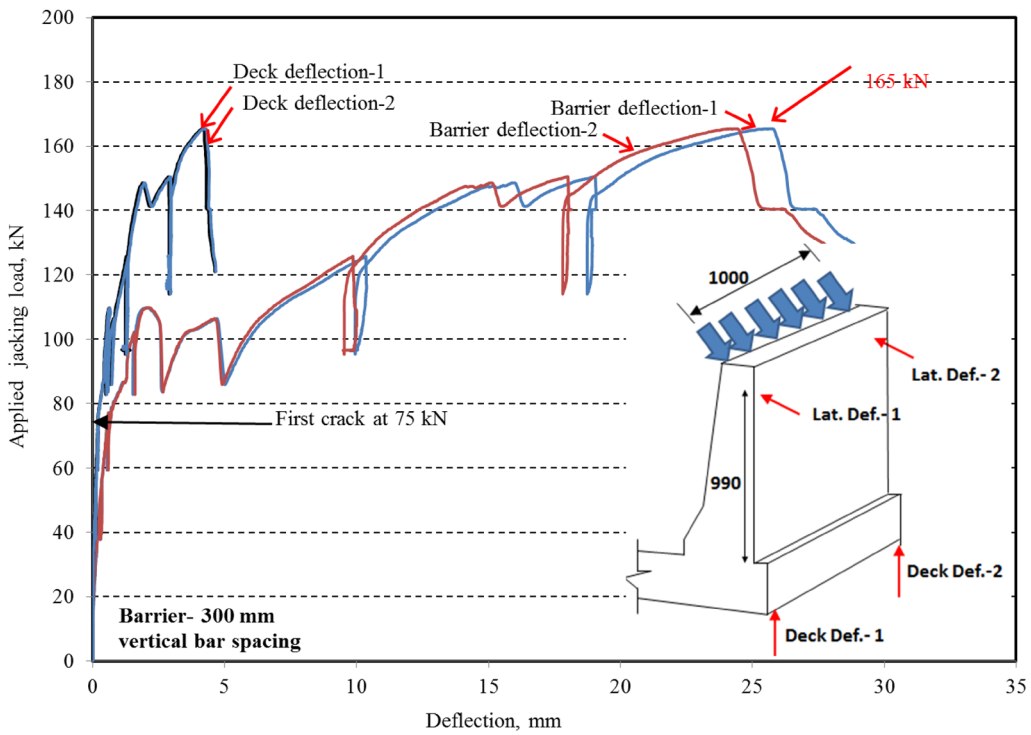

Fig. 17 Load-deflection relationship of the 1-m barrier wall at interior location.

a factor of safety of 1.15 with 0.75 resistance factor. As such, the proposed barrier details shown in Fig. 2 are considered adequate for barrier–deck anchorage at interior location where vertical bar spacing is 300 mm.

4.5 Location 5: 1000 mm Cantilever Wall at End Location

Figure 18 shows views of the crack pattern in the cantilever wall at end location after failure. It can be observed that the first visible flexural crack appeared at the front side of the barrier–deck junction at 85 kN jacking load.

Fig. 18 Crack pattern in the 1000 mm length barrier wall at exterior location. **a** Left side, **b** right side, **c** front side.

The second flexural crack appeared at 100 kN load along the intersection of the two tapered portions of the barrier front face. These cracks propagated through barrier thickness with increase in the applied load. Also, other flexural cracks appeared at the top tapered portion of the barrier front face and propagated through the barrier wall thickness with load increase. When the applied load reached 125 kN, extensive cracks appeared in deck slab portion under the barrier wall due to diagonal compression till failed at 189.5 kN. However, the main cause of failure was due the anchorage breakage of steel anchors between the deck cantilever and the concrete foundation wall. This was observed through a wide crack appearing in the asphalt layer at this location and a big noise when anchor breakage occurred, as shown in Fig. 18a. Figure 19 depicts the load–deflection history of the tested wall. One may not consider the importance of the deflection of the barrier and the deck since the design check at the barrier–deck junction is at the ultimate limit state.

The test was intended to examine the flexural capacity of the barrier wall at the bottom of the barrier as well as the anchorage capacity of the barrier–deck junction at end location where vertical bar spacing is 150 mm. Test results showed that the failure load was 189.5 kN. As such, the associated flexural capacity of the barrier wall junction or anchorage capacity is taken as 189.5 kN × 0.99 m applied load arm to the deck slab = 187.61 kN m/m. According to CHBDC of 2006 at end portion of PL-3 barrier, the factored applied moment at the barrier deck junction is 102 kN m/m. This leads to factors of safety in design equal to 1.84 and 1.38 with resistance factors of 1 and 0.75, respectively. However, considering Eq. 4, the factored applied moment at the barrier–deck junction is 142.37 kN m/m, leading to factors of safety of 1.32 and 1.0 with 1.0 and 0.75 resistance factors, respectively. As such, the proposed barrier details shown in Fig. 2 is considered adequate for barrier–deck anchorage at end location where vertical bar spacing is 150 mm. Summary of test results and associated factors of safety in design are shown in Table 1.

5 Analytical Investigation of Punching Shear Strength of PL-3 GFRP-Reinforced Barriers

Since the primary failure mode of the tested barrier at the interior and end locations is due punching shear, a punching shear strength equation is required to qualify PL-3 barrier wall design. This section intends to correlate the experimental findings with the available punching shear strength equations in the literature. Due to differences in mechanical properties of steel and GFRP bars, punching shear equations derived for steel-reinforced concrete structures cannot be employed directly to the GFRP-reinforced elements. Most of the current code provisions and empirical equations predicting punching shear strength of FRP-reinforced structures are modified forms of those available for steel-reinforced concrete structures to account for lower modulus of elasticity of FRP bars compared to steel bars. Experimental tests have shown that FRP-reinforced concrete member experienced reduced shear strength compared to steel-reinforced structures due to lower modulus of elasticity of FRP bars. The lower modulus of elasticity in turn results in larger deformation and developing wider and deeper cracks. In two-way

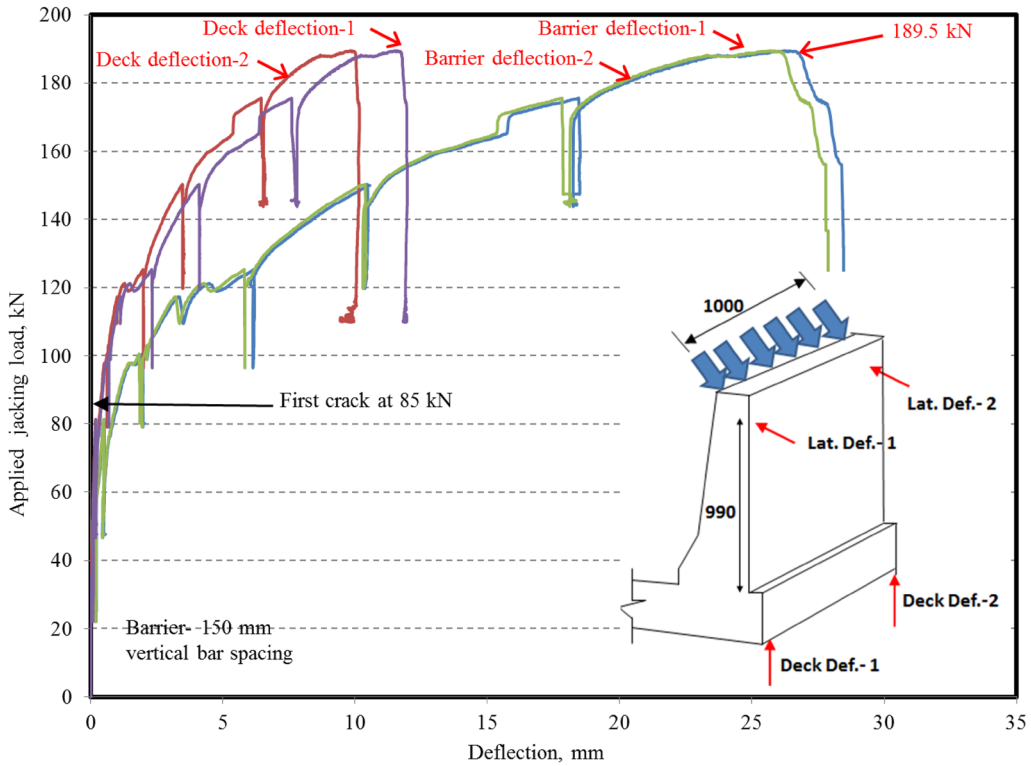

Fig. 19 Load-deflection relationship of the 1-m barrier wall at exterior location.

reinforced concrete slabs, punching shear resistance is provided by the shear resistance of concrete in the compression zone, V_c. The shear resistance acts over an area equal to the critical perimeter, b_o, of punching shear failure plane multiplied by effective depth, d, of the concrete section. The critical perimeter, b_o, is specified in different design codes as either 0.5d or 1.5d.

Previous research performed on shear capacity of FRP-reinforced flexural concrete members without shear reinforcement proved that slab shear strength is affected by stiffness of tensile (flexural) reinforcements (Nagasaka et al. 1993; Zhao et al. 1995; JSCE 1997; Sonobe 1997; Michaluk et al. 1998; Tureyen and Frosch 2002, 2003). Consequently, the FRP design codes, CSA-S806-12 (CSA 2012), ACI 440-1R-06 (2006) and JSCE Guidelines (1997) and other empirical punching shear equations developed by researchers (El-Ghandour et al. 1999, 2000, Matthys and Taerwe 2000, Ospina et al. 2003, El-Gamal et al. 2005 and Jacobson et al. 2005) considered the FRP flexural reinforcement ratio in calculating punching shear strength of FRP-reinforced concrete slabs. The following punching shear models have been selected to predict the punching shear capacities of barrier wall, which can then be compared to the test ultimate punching shear loads.

The Canadian Standard CSA S806-12 (2012) specifies the punching shear strength of FRP-reinforced concrete as the smallest of the following three equations. It can be noticed that these equations are the modified forms of those specified in the Canadian Standard CSA-A23.3-04 (2004) to account for the FRP-reinforcing bar ratio.

$$V_c = (1 + 2/\beta_c) \cdot 0.028\lambda\varphi_c \left(E_f \cdot \rho_f \cdot f'_c\right)^{1/3} \cdot b_{o,0.5d} \cdot d \quad (5)$$

$$V_c = \left[\left(\alpha_s \cdot d/b_{o,0.5d}\right) + 0.19\right] \cdot 0.147\lambda\varphi_c \left(E_f \cdot \rho_f \cdot f'_c\right)^{1/3} \cdot b_{o,0.5d} \cdot d \quad (6)$$

$$V_c = 0.056\lambda\varphi_c \left(E_f \cdot \rho_f \cdot f'_c\right)^{1/3} \cdot b_{o,0.5d} \cdot d \quad (7)$$

where, β_c is the ratio of long side to short side of the concentrated load or loading patch, λ is a density factor (i.e. for normal density concrete is equal to 1), ϕ_c is the concrete resistance factor, E_f is modulus of elasticity of FRP bars, ρ_f is the FRP tensile reinforcement ratio, f'_c is the concrete compressive strength in MPa, $b_{o,0.5d}$is the critical perimeter length measured at 0.5d from the loading patch, d is effective slab depth in mm and α_s is a factor to adjust V_c for support dimensions that is equal to 4 for

interior columns, 3 for edge columns and 2 for corner columns.

The American Standard ACI 440.1R-06 (2006) specifies the equation below for calculating punching shear capacity of FRP-reinforced concrete slab.

$$V_c = (5k/2)0.33 \cdot \sqrt{f'_c} \cdot b_{o,0.5d} \cdot d \quad (8)$$

where, $k = \left[\sqrt{2\rho_f n_f + (\rho_f n_f)^2} - \rho_f \cdot n_f\right]$ and n_f is modular ratio equal to (E_f/E_c).

The Japanese Standard (JSCE 1997) specifies that the punching shear strength can be determined from the following equation;

$$V_c = \beta_d \cdot \beta_p \cdot \beta_r \cdot \left(f_{pcd}/\gamma_b\right) \cdot b_{o,0.5d} \cdot d \quad (9)$$

where, $\beta_d = \sqrt[4]{\frac{1000}{d}} \le 1.5$ (d in mm), $\beta_p = (100\rho_f E_f/E_s)^{1/3} \le 1.5$, $\beta_r = 1 + \frac{1}{\left[1+0.25\left(\frac{u_0}{d}\right)\right]}$; u_0 is the perimeter of concentrated load area, $f_{pcd} = 0.2\sqrt{f'_c} \le 1.2$ in MPa and γ_b is a partial safety factor to account for concrete compressive strengths below 50 MPa (1.3) and above 50 MPa (1.5). However, γ_b is set equal to 1 to determine an un-factored prediction capacity to be compared with experimental ultimate strength.

From the experimental tests performed on FRP-reinforced flat slabs, El-Ghandour et al. (1999) proposed a modification to the punching shear strength specified in the ACI code ACI-318-05 (ACI318 2005) by applying the term $(E_f/E_s)^{1/3}$ to the predicted punching shear strength as follow

$$V_c = 0.33\sqrt{f'_c} \cdot (E_f/E_s)^{1/3} b_{o,0.5d} \cdot d \quad (10)$$

El-Ghandour et al. (2000) proposed a modification to the British Code BS 8110-1 (British Standard Institution 2002) by applying strain correction factor $(0.0045/\varepsilon_y)$ to the equivalent reinforcement ratio ($\rho_s = \rho_f \cdot E_f/E_s$) so that a strain limit of 0.0045 is assumed for FRP reinforcements. ε_y is the yield strain of steel reinforcements typically equal 0.002. Therefore, El-Ghandour et al. proposed the following equation to determine the punching shear strength of FRP-reinforced concrete slabs.

$$V_c = 0.79\left[100\rho_f(E_f/E_s) \cdot \left(0.0045/\varepsilon_y\right)\right]^{1/3} \cdot (f_{cu}/25)^{1/3}(400/d)^{1/4} b_{o,1.5d} \cdot d \quad (11)$$

where, f_{cu} is the concrete cube strength equal to ($f_{cu} = f'_c/0.8$ MPa) and $b_{o,1.5d}$ is the critical perimeter length measured at a distance 1.5d away from the loading patch.

Matthys and Taerwe (2000) conducted experimental study on punching shear strength of concrete slabs reinforced with FRP grids. From experimental investigations, they proposed the following modification to the provisions of BS-8110-1 Standard (2002) to account for the use of FRP bars.

$$V_c = 1.36[100\rho_f(E_f/E_s)]^{1/3}\left(f'_c\right)^{1/3}(1/d)^{1/4} \cdot b_{o,1.5d} \cdot d \quad (12)$$

Ospina et al. (2003) performed experimental tests on flat slabs reinforced with FRP bars and grids and proposed a modification to the punching shear strength suggested by Matthys and Taerwe (2000) as follow.

$$V_c = 2.77\left(\rho_f f'_c\right)^{1/3}(E_f/E_s)]^{1/2} b_{o,1.5d} \cdot d \quad (13)$$

El-Salakawy et al. (2005) proposed modification to the ACI318-05 (2005) punching shear equation by applying a new parameter (α) as follows.

$$V_c = 0.33\sqrt{f'_c} \cdot b_{o,0.5d} \cdot d \cdot \alpha \quad (14)$$

where, $\alpha = 0.5(\rho_f E_f)^{1/3} \cdot (1 + 8d/b_{o',0.5d})$ and E_f is in GPa.

Jacobson et al. (2005) conducted experimental investigation on punching shear capacity of double layer FRP grid-reinforced slabs and proposed a new model which is a modification of the empirical approach suggested by Matthys and Taerwe (2000) as follows.

$$V_c = 4.5\left(\rho_f f'_c\right)^{1/3} \cdot (1/d)^{1/4} \cdot b_{o,1.5d} \cdot d \quad (15)$$

where, ρ_f is to be calculated as the average of the two reinforcement ratios in both longitudinal and transverse directions.

All above-mentioned prediction models consider the reinforcement ratio of tension reinforcement in the direction of applied tension force for edge loading, except JSCE-1997 and Jacobson el al. that consider the average reinforcement ratios in both directions at tension face of slab. The punching shear strength of the developed GFRP-reinforced PL-3 barrier in this study was calculated using various equations mentioned earlier at the interior and exterior locations shown in Fig. 4a. Table 2 provides the predicted capacities of the PL-3 barrier in accordance with above-mentioned punching shear equations, V_c, along with the ratio between the experimental and predicted punching shear strength ($V_{c,exp}/V_c$). Traditionally, the $V_{c,exp}/V_c$ ratio of 1 presents perfectly predicted test capacity, while ratios greater than 1 provide conservatism

Table 2 Punching shear capacities of the tested GFRP-reinforced PL-3 bridge barriers using available design codes and previous research.

References to punching shear capacity equations	Interior location ($V_{c,\ exp} = 621$ kN)			End location ($V_{c,exp} = 593$ kN)		
	V_c	$V_{c,exp}/V_c$ ratio[a]	$V_{c,exp}/V_c$ ratio[b]	V_c	$V_{c,exp}/V_c$ ratio[a]	$V_{c,exp}/V_c$ ratio[b]
CSA-S806-12 (2012), ($V_{c,\ S806}$)	323.2	1.88	*1.41*	350.8	1.69	*1.27*
ACI 440.1R-06 (2006), ($V_{c,\ ACI\ 440}$)	371.5	1.63	*1.23*	440.6	1.35	*1.01*
JSCE (1997), ($V_{c,\ JSCE}$)	649.4	0.93	0.70	715.0	0.83	0.62
El-Ghandour et al. (1999), ($V_{c,\ EGA\ 1999}$)	869.8	0.70	0.52	749.9	0.79	0.59
El-Ghandour et al. (2000), ($V_{c,\ EGA\ 2000}$)	568.0	1.07	0.80	564.8	1.05	0.79
Matthys and Taerwe (2000), ($V_{c,\ MT}$)	452.9	1.34	*1.01*	450.4	1.32	*0.99*
Ospina et al. (2003), ($V_{c,\ OSP}$)	621.2	0.98	0.73	617.7	0.96	0.72
El-Gamal et al. (2005), ($V_{c,\ EGM}$)	561.5	1.08	0.81	642.0	0.92	0.69
Jacobson et al. (2005), ($V_{c,\ JCOB}$)	512.1	1.19	0.89	452.3	1.31	0.98

[a] Considering resistance factor = 1.

[b] Considering resistance factor = 0.75.

in designing punching shear capacity of the barrier walls. Ratios less than 1 show that the predicted punching shear models overestimate the experimental shear capacity of the barrier walls making the design unsafe. From the punching shear prediction models reported in Table 2, the predication by CSA-S806-12, ACI 440.1R-06 and Mattys and Taerwe's equations resulted in factors of safety of 1.41, 1.23 and 1.01 at interior location and 1.27, 1.01 and 0.99 at end location, respectively. Other equations presented in Table 2 provided unsafe prediction of the barrier punching strength at interior and end locations of the proposed PL-3 barrier.

6 Conclusions

A cost-effective GFRP bar arrangement was proposed for PL-3 barrier wall and barrier–deck slab junction incorporating high-modulus GRRP bars with headed ends. Based on the experimental findings and analytical investigation, the following conclusions can be drawn.

1. In contrast to AASHTO-LRFD yield-line failure pattern specified for steel-reinforced barriers, the developed GFRP-reinforced barrier wall failed due to punching shear around the patch load location.
2. Considering a resistance factor of 0.75 to experimental results, the developed GFRP-reinforced barrier exhibited ultimate load carrying capacities far greater than the CHBDC design load with factors of safety of 1.25 and 1.28 for interior and exterior load locations, respectively.
3. Considering a resistance factor of 0.75 to experimental results, the developed GFRP-reinforced barrier exhibited anchorage capacities at the barrier–deck junction for the 360 mm thick deck slab cantilever of 1 m length with factors of safety of 1.15 and 1.0 at interior and end locations, respectively.
4. From the punching shear prediction models available in the literature, the predication by CSA-S806-12, ACI 440.1R-06 and Mattys and Taerwe's equations resulted in factors of safety of 1.41, 1.23 and 1.01 at interior location and 1.27, 1.01 and 0.99 at end location, respectively, considering factor of safety of 0.75. Other punching shear equations provided unsafe prediction of the barrier punching strength at interior and end locations of the proposed PL-3 barrier.
5. Based on the experimental findings, it is recommended replacing Figure C16.2 in the 2014 CHBDC Commentaries (which is identical to Fig. 2a in this paper) with the proposed PL-3 barrier in Fig. 2b given (i) the significant reduction in cost with the elimination of bar bents, (ii) the use of high-modulus GFRP bars with almost double the tensile strength of GFRP bars specified in Figure C16.2, (iii) that Canadian GFRP manufacturers and suppliers currently produce high-modulus bars with guaranteed tensile strength more than 1000 MPa in contrast to the outdated low-modulus GFRP bars, and (vi) that the proposed design reduces the amount of GFRP bars in the barrier detailing in Figure C16.2 by about 43%.

Authors' contributions

The authors shared carrying out this research and writing this paper. All authors read and approved the final manuscript.

Author details

[1] Civil Engineering Department, Ryerson University, 350 Victoria Street, Toronto, ON M5B 2K3, Canada. [2] Structural Engineering Department, Alexandria University, 22 El-Guish Road, El-Shatby, Alexandria 21526, Egypt. [3] Civil Engineering and Construction Department, Georgia Southern University, Engineering Building, Room 1101G, 201 COBA Drive, BLDG 232, Statesboro, GA 30458, USA.

Acknowledgements
The authors acknowledge the support to this project by Schoeck Canada Inc. of Kitchener, Ontario, Canada. Also, the authors would like to thank Mr. Nidal Jaalouk, Lead Technical Officer at Ryerson University, for assisting in barrier instrumentation and conducting the tests.

Competing interests
The authors declare that they have no competing interests.

Publisher's Note

Received: 7 February 2017 Accepted: 26 June 2018
Published online: 03 October 2018

References

AASHTO. (2009). *AASHTO-LRFD Bridge Guide Specifications for GFRP-Reinforced Concrete Bridge Decks and Traffic Railings*. Washington, D.C.: American Association of State Highway and Transportation Officials.

AASHTO. (2012). *AASHTO-LRFD Bridge Design Specifications* (3rd ed.). Washington, DC: American Association of State Highway and Transportation Officials.

ACI. (2002). *440.2R-02 Guide for the design and construction of externally bonded FRP systems for strengthening concrete structures: 45*. Farmington Hills, Michigan: American Concrete Institute.

ACI. (2006). *440.1R-06. Guide for the design and construction of structural concrete reinforced with FRP bars*. Farmington Hills, MI, USA: American Concrete Institute.

ACI318. (2005). *Building Code Requirements for Structural Concrete (ACI 318-05), and Commentary (ACI 318R-05)*. Farmington Hills, MI, USA: American Concrete Institute.

Azimi, H., Sennah, K., Sayed-Ahmed, M., Nikravan, N., Louie, J., Hassaan, A., et al. (2014a). Bridge deck-guardrail anchorage detailing for sustainable construction. *ASCE Journal of Bridge Engineering, 19*(10), 1–12.

Azimi, H., Sennah, K., Tropynina, E., Goremykin, S., Lucic, S., & Lam, M. (2014b). Anchorage capacity of concrete bridge barriers reinforced with GFRP bars with headed ends. *ASCE Journal of Bridge Engineering, 19*(9), 1–15.

British Standard Institution. (2002). Part 1: Code of Practice for Design and Construction. BS 8110- 1: 1997 Structural Use of Concrete, London, UK.

Buth, C., William, W., Bligh, R., Menges, W., & Haug, R. (2003). Performance of the TxDOT T202 (MOD) bridge rail reinforced with reinforced polymer bars. Report No. FHWA/TX-03/0-4138-3, *Texas Transportation Institute*. College Station, Texas.

Charron, J., Niamba, E., & Massicotte, B. (2011). Static and dynamic behavior of high- and ultrahigh-performance fiber-reinforced concrete precast bridge parapets. *ASCE Journal of Bridge Engineering, 16*(3), 413–421.

CSA. (2004). Design of Concrete Structures, CSA-A23.3-04. In*Canadian Standards Associations*. Mississauga, Ontario, Canada.

CSA. (2006a). Canadian Highway Bridge Design Code. In *Canadian Standard Association*, Toronto, Ontario, Canada.

CSA. (2006b). Commentaries on the Canadian Highway Bridge Design Code, CAN/CSA-S6-06. In *Canadian Standard Association*, Toronto, Ontario, Canada.

CSA. (2012). *Design and Construction of Building Structures with Fibre Reinforced Polymers, CSA-S806-12*. Toronto, Ontario: Canadian Standards Association.

CSA. (2014a). Canadian Highway Bridge Design Code, CAN/CSA-S6-14. In *Canadian Standard Association*. Toronto, Ontario, Canada.

CSA. (2014b). Commentaries on the Canadian Highway Bridge Design Code, CAN/CSA-S6-14. In *Canadian Standard Association*. Toronto, Ontario, Canada.

El-Gamal, S., El-Salakawy, E., & Benmokrane, B. (2005). A new punching shear equation for two-way concrete slabs reinforced with FRP bars. *ACI Special Publication, SP, 230–50,* 877–894.

El-Ghandour, A., Pilakoutas, K., & Waldron, P. (1999). New approach for punching shear capacity prediction of fiber reinforced polymer reinforced concrete flat slabs. *ACI Journal, SP, 188–13,* 135–144.

El-Ghandour, A., Pilakoutas, K., & Waldron, P. (2000). Punching shear behavior and design of FRP RC flat slabs. *Proceedings of the international workshop on punching shear capacity of RC slab, Stockholm: TRITA-BKN Bulletin, 57,* 359–366.

El-Gamal, S., Tobbi, H., El-Sayed, A., & Benmokrane, B. (2007). *Impact Testing of Concrete Bridge Barriers Reinforced with New GFRP Bars (Types 201 and 301)*. Canada: Technical Report, Ministry of Transportation of Quebec.

El-Salakawy, E., Benmokrane, B., Masmoudi, R., Brière, F., & Breaumier, E. (2003). Concrete bridge barriers reinforced with glass fiber-reinforced polymer composite bars. *ACI Structural Journal, 100*(6), 815–824.

El-Salakawy, E., & Islam, M. (2014). Repair of GFRP-reinforced concrete bridge barriers. *ASCE Journal of Bridge Engineering, 19*(6), 1–11.

El-Salakawy, E., Masmoudi, R., Benmokrane, B., Briére, F., & Desgagné, G. (2005). Pendulum impacts into concrete bridge barriers reinforced with GFRP composite bars. *Canadian Journal of Civil Engineering, 31*(4), 539–552.

Hedjazi, S., Khederzadeh, H., & Sennah, K. (2016). Numerical modeling for structural behavior of bridge deck barriers made of fiber reinforced concrete. In *Proceedings of the 5th International Structural Specialty Conference*. Canadian Society for Civil Engineering, London, Ontario, Canada.

Jacobson, D., Bank, L., Oliva, M., & Russell, J. (2005). Punching shear capacity of double layer FRP grid reinforced slabs. *ACI Special Publication, SP, 230–49,* 857–875.

JSCE. (1997). Recommendation for design and construction of concrete structures using continuous fiber reinforcing materials. *Japan Society of Civil Engineers*, Concrete Engineering Series No. 23 (p. 325).

Karbhari, VM. (2000). Determination of Materials Design Values for the Use of Fibre-Reinforced Polymer Composites in Civil Infrastructure. In *Proceedings of the Institution of Mechanical Engineers—Materials and Design*. 214 (Part L) (pp. 163–171).

Khederzadeh, H., & Sennah, K. (2014). Development of cost-effective PL-3 concrete bridge barrier reinforced with sand-coated GFRP bars: static load tests. *Canadian Journal for Civil Engineering, 41*(4), 368–379.

Khederzadeh, H., & Sennah, K. (2015). Finite-element modeling of bridge barrier walls reinforced with GFRP bars and subjected to equivalent transverse impact loading. In *Proceedings of the 4th Specialty Conference on Material Engineering and Applied Mechanics*. CSCE, Regina, SK, Canada.

Lai, D., & Raven, R. (2010). Performance of epoxy coated reinforcement in bridge barriers subjected to direct salt splashing. In *Proceedings of the 8th International Conference on Short and Medium Span Bridges* (pp. 424–434). Niagara Falls, Ontario, Canada.

Maheu, J., & Bakht, B. (1994). A new connection between concrete barrier walls and bridge decks. In *Proceedings of the CSCE Annual Conference* (pp. 224-229) Winnipeg, Manitoba, Canada.

Manning, D. (1996). Corrosion performance of epoxy-coated reinforcing steel: north american experience. *Journal of Construction and Building Materials., 10*(5), 349–365.

Matta, F., & Nanni, A. (2009). Connection of concrete railing post and bridge deck with internal FRP reinforcement. *ASCE Journal of Bridge Engineering, 14*(1), 66–76.

Matthys, S., & Taerwe, L. (2000). Concrete slabs reinforced with FRP Grids, Part II: punching resistance. *ASCE Journal of Composites for Constructions, 4*(3), 154–161.

Michaluk, C., Rizkalla, S., Tadros, G., & Benmokrane, B. (1998). Flexural behavior of one-way concrete slabs reinforced by fiber reinforced plastic reinforcement. *ACI Structural Journal, 95*(3), 353–364.

Nagasaka, T., Fukuyama, H., & Tanigaki, M. (1993). Shear performance of concrete beams reinforced with FRP stirrups. *Fiber-Reinforced-Plastic Reinforcement for Concrete Structures—International Symposium*, SP-138, A.

Ospina, C., Alexander, S., & Cheng, R. (2003). Punching of two-way concrete slabs with fiber-reinforced polymer reinforcing bars or grids. *ACI structural Journal, 100*(5), 589–598.

Rostami, M., Sennah, K., & Dehnadi, S. (2016). Experimental study on the capacity of barrier–deck anchorage in MTQ PL-3 barrier reinforced with HM-GFPP bars with headed ends. In *Proceedings of the 5th International Structural Specialty Conference, Canadian Society for Civil Engineering*. London, Ontario, Canada.

SchÖck Canada Inc. (2010). GFRP Bar Data Sheet. http://www.Schoeck-canada.com.

Sennah, K., Juette, B., Weber, A., & Witt, C. (2011). Vehicle crash testing on a GFRP-reinforced concrete bridge barrier. In *Proceedings of the Annual*

Conference of the Transportation of Canada (TAC) (pp. 11–14). Edmonton, Alberta, Canada.
Sennah, K., & Khederzadeh, H. (2014). Development of cost-effective PL-3 concrete bridge barrier reinforced with sand-coated GFRP bars: vehicle crash test. *Canadian Journal for Civil Engineering, 41*(4), 357–367.
Smith, J., & Virmani, Y. (1996). Performance of epoxy-coated rebars in bridge decks. *Public Roads Magazine, 60*(2), 1–12.
Sonobe, Y. (1997). Design guidelines of FRP reinforced concrete building structures. *Journal of Composites for Constructions, 1*(3), 90–115.
Tureyen, A., & Frosch, R. (2002). Shear tests of FRP reinforced concrete beams without stirrups. *ACI Structural Journal, 99*(4), 427–434.
Tureyen, A., & Frosch, R. (2003). Concrete shear strength: another perspective. *ACI Structural Journal, 100*(5), 609–615.
Zhao, W., Maruyama, K., & Suzuki, H. (1995). Shear behavior of concrete beams reinforced by FRP rods as longitudinal and shear reinforcement. In *Proceedings of the Second International RILEM Symposium on Non-Metallic (FRP) Reinforcement for Concrete Structures (FRPRCS-2)*, Ghent, Belgium, 352-359.